SUPPLEMENTAL FIGURES, TABLES, AND EXPERIMENTAL PROCEDURES

Supplementary Table 1. Basic intrinsic properties of normal and deprived PV neurons examined before and during bath NRG1.

		Number of neurons	Resting membrane potential (mV)	Input resistance (MΩ)	Rheobase (current strength, pA)	Spike height (mV)
Normal PV neurons	Control	16	-65 ± 1.1	185.9 ± 17.3	104.7 ± 13.9	89.7 ± 2.8
	NRG1	12	-65.4 ± 1.2	186 ± 22	102.1 ± 19	87.1 ± 3.3
Deprived PV neurons	Control	14	-62.9 ± 1.1	180 ± 9	114.3 ± 14	95.2 ± 2.5
	NRG1	13	-63 ± 1.2	183.2 ± 8.5	111.5 ± 14.3	94 ± 2.9

Supplementary Table 2. NRG1 treatment enhances EPSC inputs to deprived PV neurons in terms of the number of detected EPSCs and their integrated amplitudes

	Pre-NRG1 control		**Bath NRG1**	
	average number of detected EPSCs	average integrated amplitude per EPSC (pA/ms)	average number of detected EPSCs	average integrated amplitude per EPSC (pA/ms)
Normal PV neurons	148 ± 41.8	6.14 ± 0.43	140 ± 38	6.7 ± 0.54
MD PV neurons	50 ± 15.3	5.3 ± 0.43	156 ± 39.5 *	6.91 ± 0.61 *

	Repeated injection for 48 hours		**single injection, 1 hour**	
	average number of detected EPSCs	average integrated amplitude per EPSC (pA/ms)	average number of detected EPSCs	average integrated amplitude per EPSC (pA/ms)
MD PV neurons with *in vivo* NRG1 treatment	281.7 ± 46 ***	7.56 ± 0.41 ***	619.3 ± 148 ***	7.13 ± 0.36 *

The quantification listed in this table is related to the analysis shown in Fig. 2J of average total synaptic input strength measured for L2/3 PV neurons under the specified conditions. * indicates the significance of $p < 0.05$ while compared to control data of monocular deprived (MD) PV neurons without NRG1 treatment, and *** indicates the significance of $p < 0.001$.

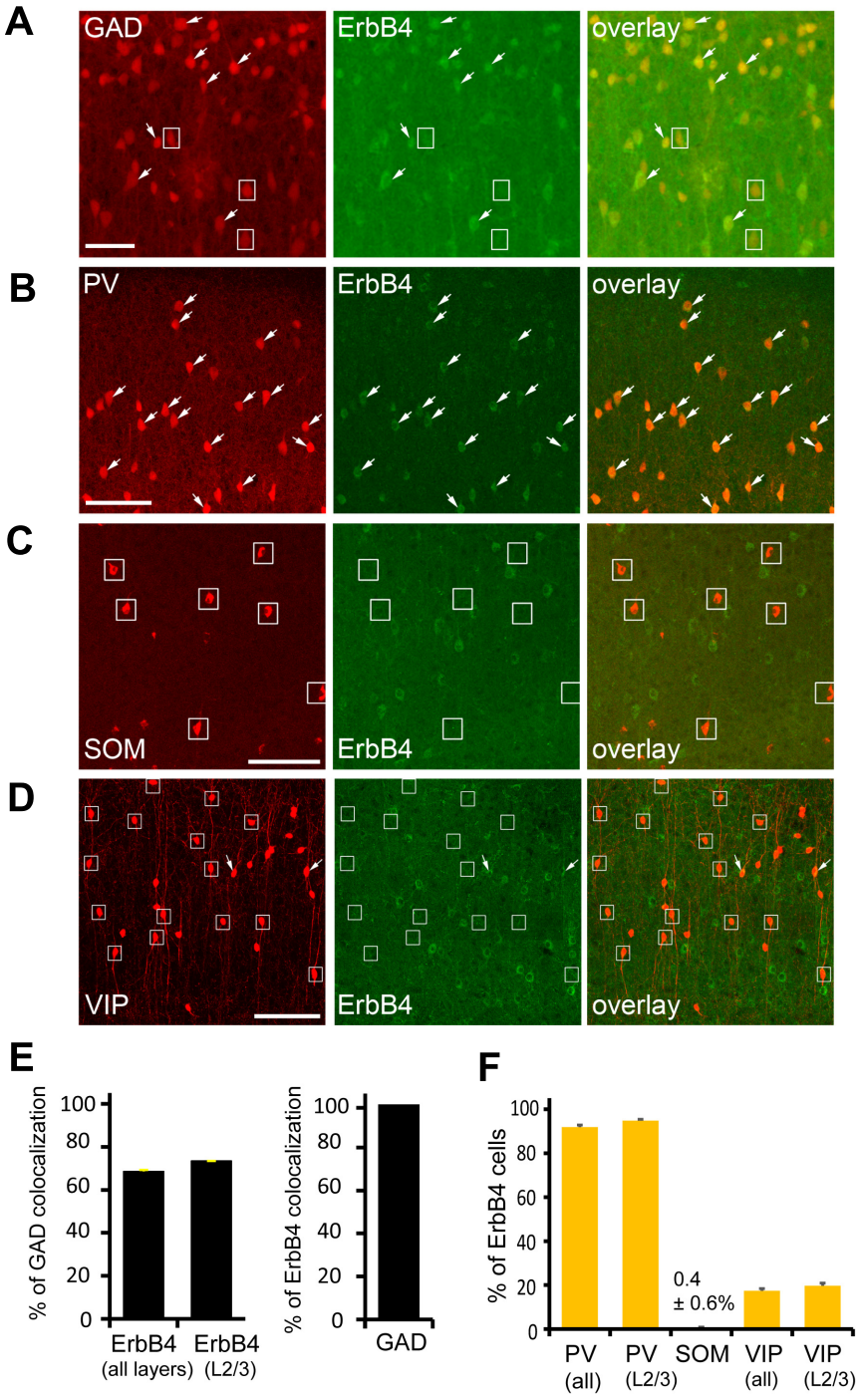

Supplementary Figure 1. ErbB4 expression occurs in a subset of GABAergic cells, and is largely restricted to PV neurons in mouse visual cortex during the critical period.

A, Representative confocal images of genetically labeled GABAergic cells (red), ErbB4 immunolabeling (green) and their overlay in layer (L) 2/3 of GAD2-Cre; Ai9 mouse V1. Arrows indicate glutamate decarboxylase (GAD)-expressing cells immunopositive for ErbB4 and white squares encompass ErbB4 immuno-negative GABAergic cells. Scale = 50 μm. **B**, Representative confocal images of genetically labeled PV cells (red), ErbB4 immunolabeling (green) and their overlay in layer 2/3 of PV-Cre; Ai9 mouse V1. Nearly all PV cells are strongly immunopositive for ErbB4. **C**, Representative confocal images of immunolabeled somatostatin (SOM) cells (red), ErbB4 immunolabeling (green) and their overlay in layer 2/3 of mouse V1. Essentially no SOM cells are immunopositive for ErbB4. **D**, Representative confocal images of genetically labeled vasoactive intestinal peptide (VIP) cells (red),

ErbB4 immunolabeling (green) and their overlay in L2/3 of VIP-Cre; Ai9 mouse V1. A relatively small proportion of VIP cells are immunopositive for ErbB4, indicated with arrows. Scale = 100 μm in (**B**, **C**, **D**). **E**, Summary of the quantification of ErbB4 and GAD co-localization. All ErbB4 expressing cells are GAD positive across all cortical layers in mouse V1. Overall, 68.6 ± 0.73% (mean ± SE) of GABAergic cells across all the cortical layers are immunopositive for ErbB4, and 73.4 ± 0.03% of GABAergic cells in L2/3 are ErbB4 positive. The quantification is based on the counts of 1070 GAD+ cells pooled from 4 sections of 2 different mice. **F**, Summary of % ErbB4 expressing cells in the subtypes of inhibitory neurons. Overall, 91.9 ± 1% of PV cells are positive for ErbB4 across all the layers of mouse V1, and in L2/3, 94.8 ± 0.6% of PV cells are positive for ErbB4. The quantification is based on the counts of 1276 PV cells pooled from 6 sections of 3 different mice. The measurements from 5 sections of 2 different mice indicate that there is virtually no co-localization between SOM and ErbB4, as only 1 out of 344 SOM cells is potentially positive for ErbB4. Overall, 17.4 ± 1 % of VIP cells are positive for ErbB4 across all the layers of mouse V1, and in L2/3, 19.8 ± 1.2% of VIP cells are positive for ErbB4. The quantification is based on the counts of 283 VIP cells pooled from 3 sections of 2 different mice. The mice for the immunostaining experiments shown for this figure were used between postnatal days of 27 – 29 within the defined critical period.

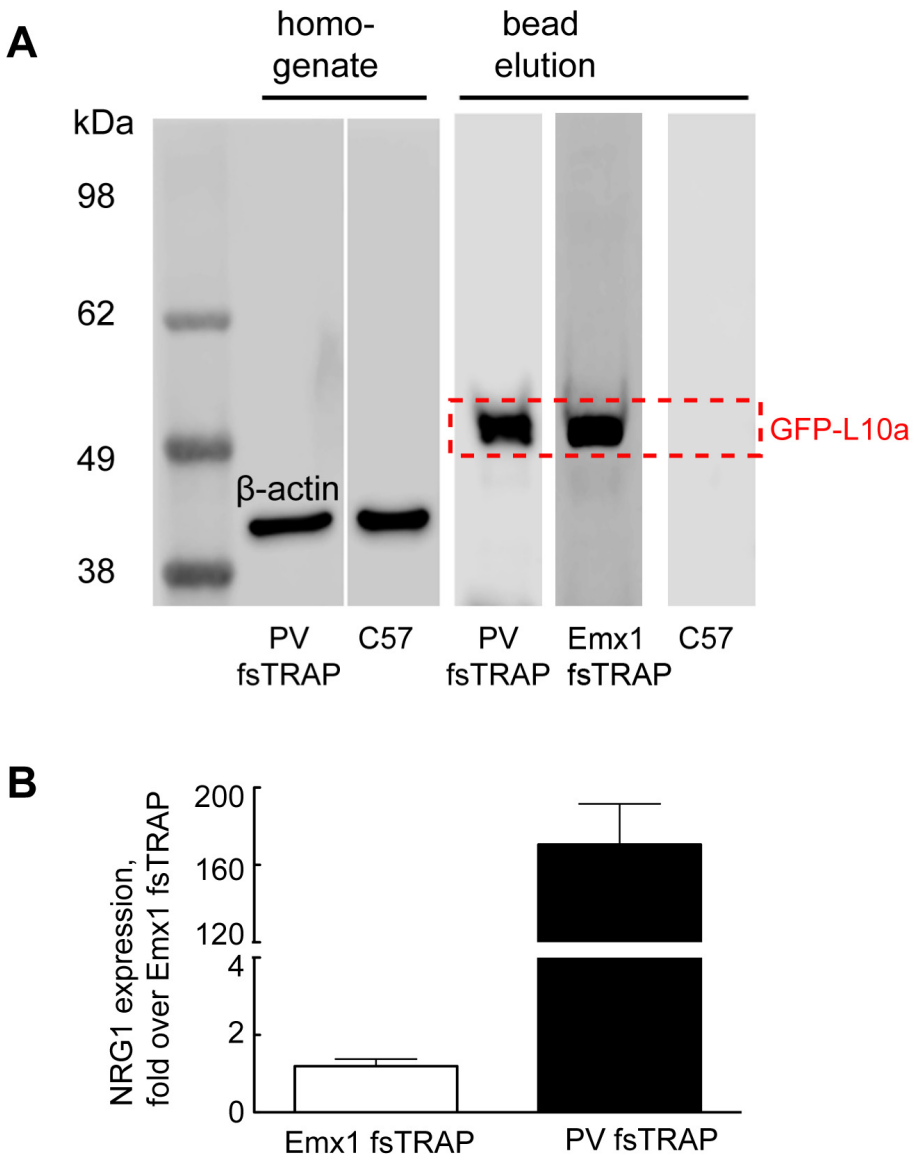

Supplementary Figure 2. Cell specific fsTRAP analysis indicates that PV neurons in the visual cortex has stronger NRG1 mRNA expression than excitatory neurons targeted by using Emx1-Cre mice.

A. Western blotting confirmation of EGFP-L10a tagged polyribosomes in PV-Cre; fsTRAP (PV fsTRAP) and Emx1-Cre; fsTRAP (Emx1 fsTRAP) mice. While both wild type C57 and PV fsTRAP cortical cell-lysate supernatants are positive for β-actin (41 kDa), only the bead elution of PV fsTRAP and Emx1 fsTRAP samples shows immunoblot of EGFP-L10a fusion protein (about 50 kDa in size). This analysis indicates the specificity of Cre-dependent expression of GFP-L10a fusion proteins in fsTRAP cells. **B**. Summary of NRG1 mRNA expression of PV fsTRAP vs Emx1 fsTRAP samples (15 and 9 samples each) using the expression fold over the average Emx1 fsTRAP value.

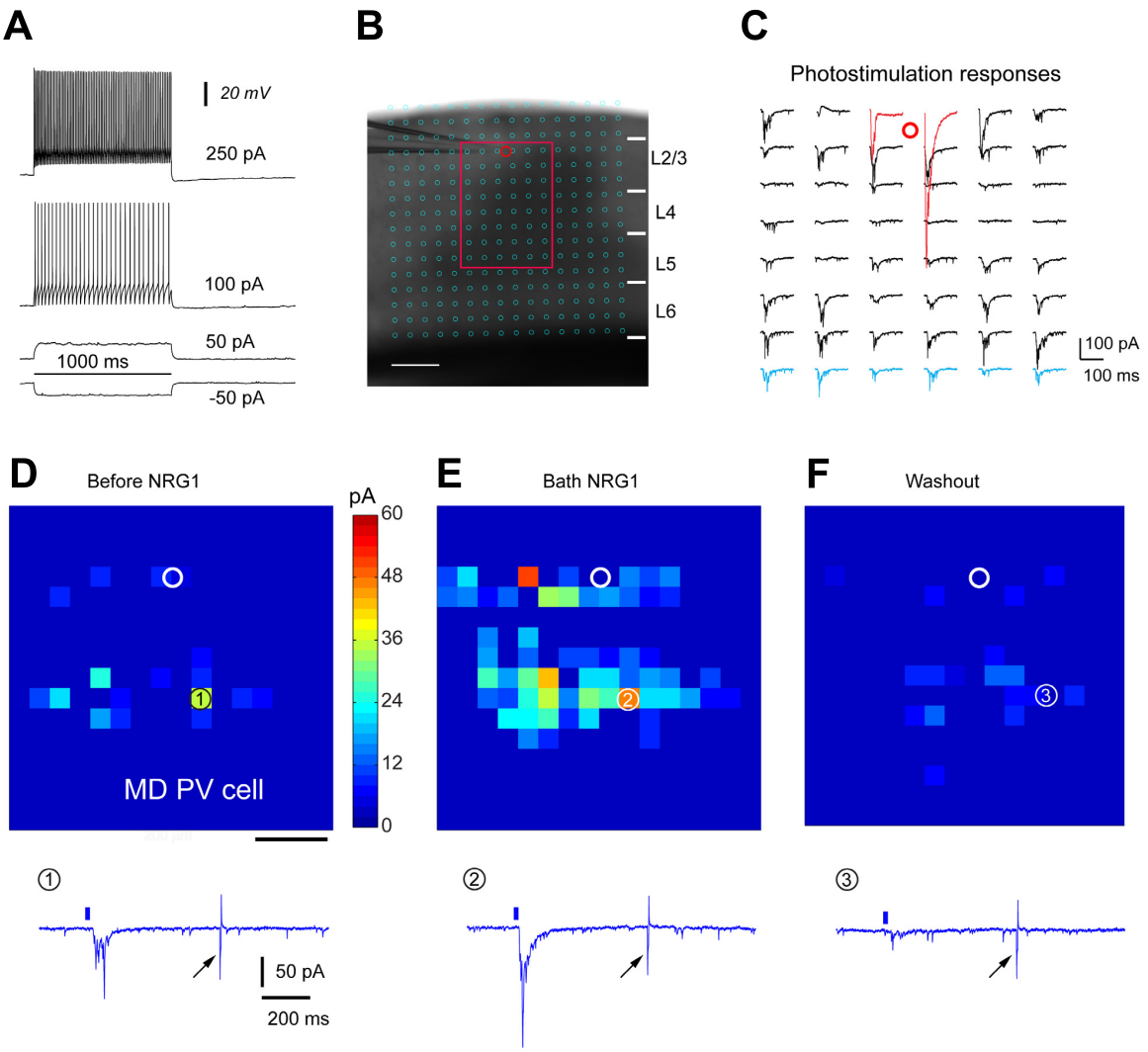

Supplementary Figure 3. Laser scanning photostimulation (LSPS) allows for quantitative and extensive mapping of local excitatory synaptic inputs to PV neurons.
A, PV/fast-spiking (FS) cells are targeted by tdTomato expression in PV-Cre; Ai9 mouse V1 slices, and verified by their typical FS firing patterns evoked by intrasomatic current injections. **B-F**, LSPS allows for extensive and quantitative analysis of synaptic inputs to recorded PV cells from laminar circuits in a relatively large cortical region. **B**, A V1 slice image superimposed with photostimulation sites (cyan circles) spaced at 60 µm x 60 µm. The red circle indicates the tip of a recording electrode and the cell body location of a recorded L2/3 monocular deprived PV neuron. Scale bar = 200 µm. **C**, The plot of excitatory postsynaptic current (EPSC) responses from the recorded PV cell at the selected sites within the region shown by the red circle in **B**, in response to photostimulation via glutamate uncaging during NRG1 bath application. The red traces indicate example direct responses, and the blue traces indicate synaptic input responses. The response traces are plotted for 200 ms beginning at the photostimulation onset. The two types of responses can be distinguished based on their waveforms, amplitudes and response latencies. The direct responses are analyzed for glutamate mediated excitability, but excluded for synaptic input analysis. The raw data as shown in **C** are quantified, and used for construction of color-coded quantitative input maps. **D-F**, Representative example of bath NRG1 enhancing synaptic input responses to a PV cell from an animal subjected to 2-day monocular deprivation. Data maps were obtained before (**D**), during (**E**) and after washout (**F**) of bath NRG1. The spatial scale beneath (**D**) indicates 200 µm. Color scale (**D)** indicates average integrated input strength at individual map sites. The warmer color indicates stronger input strength. The white circle indicates the cell body location of the monocular deprived PV neuron. Each map site (color pixel) is spaced at 60 µm x 60 µm.

Synaptic input responses at the specified, numbered sites are shown below. The response traces are plotted for 1200 ms, with 200 ms baseline before 1 ms photostimulation (blue ticks above the traces). Arrows indicate current injection responses (5 pA, 5 ms) to monitor access resistance during mapping experiments. Any recordings in which the access resistance changed by >20% during the course of the experiment were excluded from analysis.

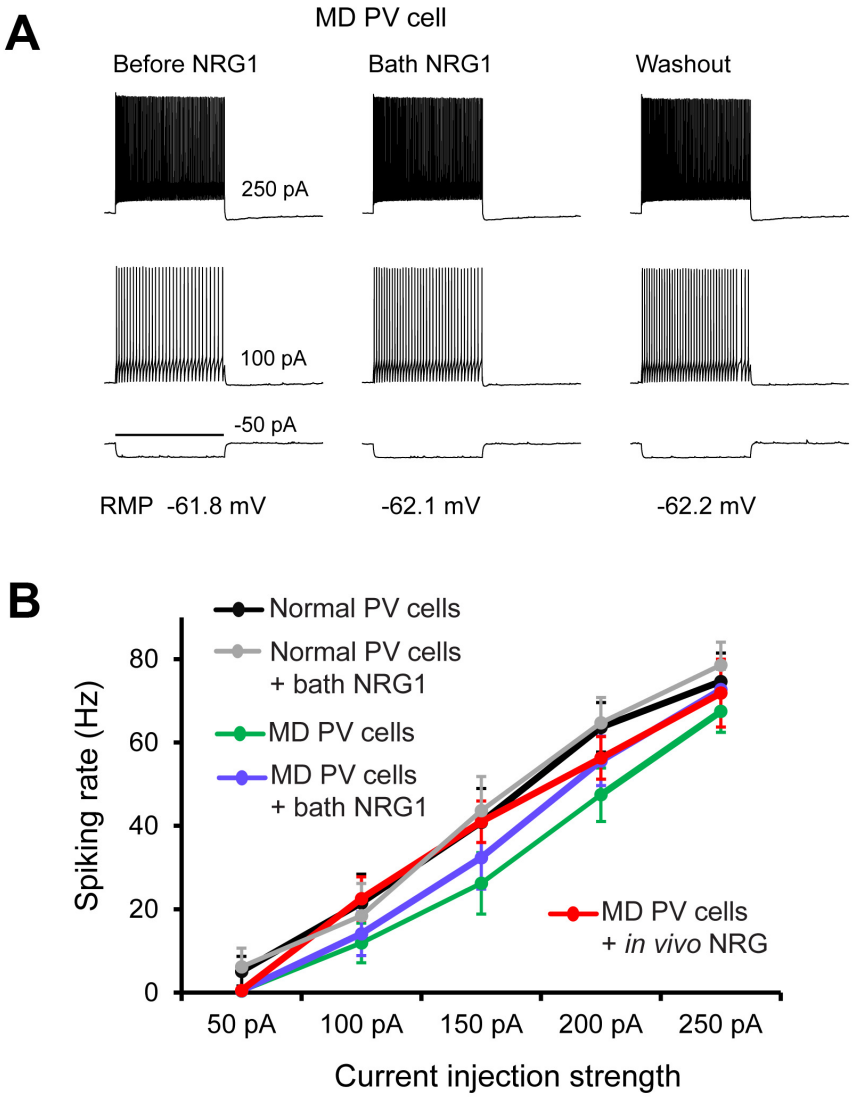

Supplementary Figure 4. Intrinsic membrane excitability of PV neurons does not change with NRG1 treatment under monocular deprivation or normal conditions.
A, Example electrophysiological responses of PV cells from animals subjected to monocular deprivation to depolarizing and hyperpolarizing, intrasomatic current injections before, during and after NRG1 bath application. **B**, The plots show the overall relationship between PV cell spiking rates and current injection strengths from control and monocular deprived animals with and without NRG1 treatment. The data values are represented mean ± SEM, with 14 normal PV cells, 13 deprived PV cells with NRG1 bath application, and 12 deprived PV cells with *in vivo* NRG1 treatment, respectively. There is no significant difference between the plotted data points at each current injection strength.

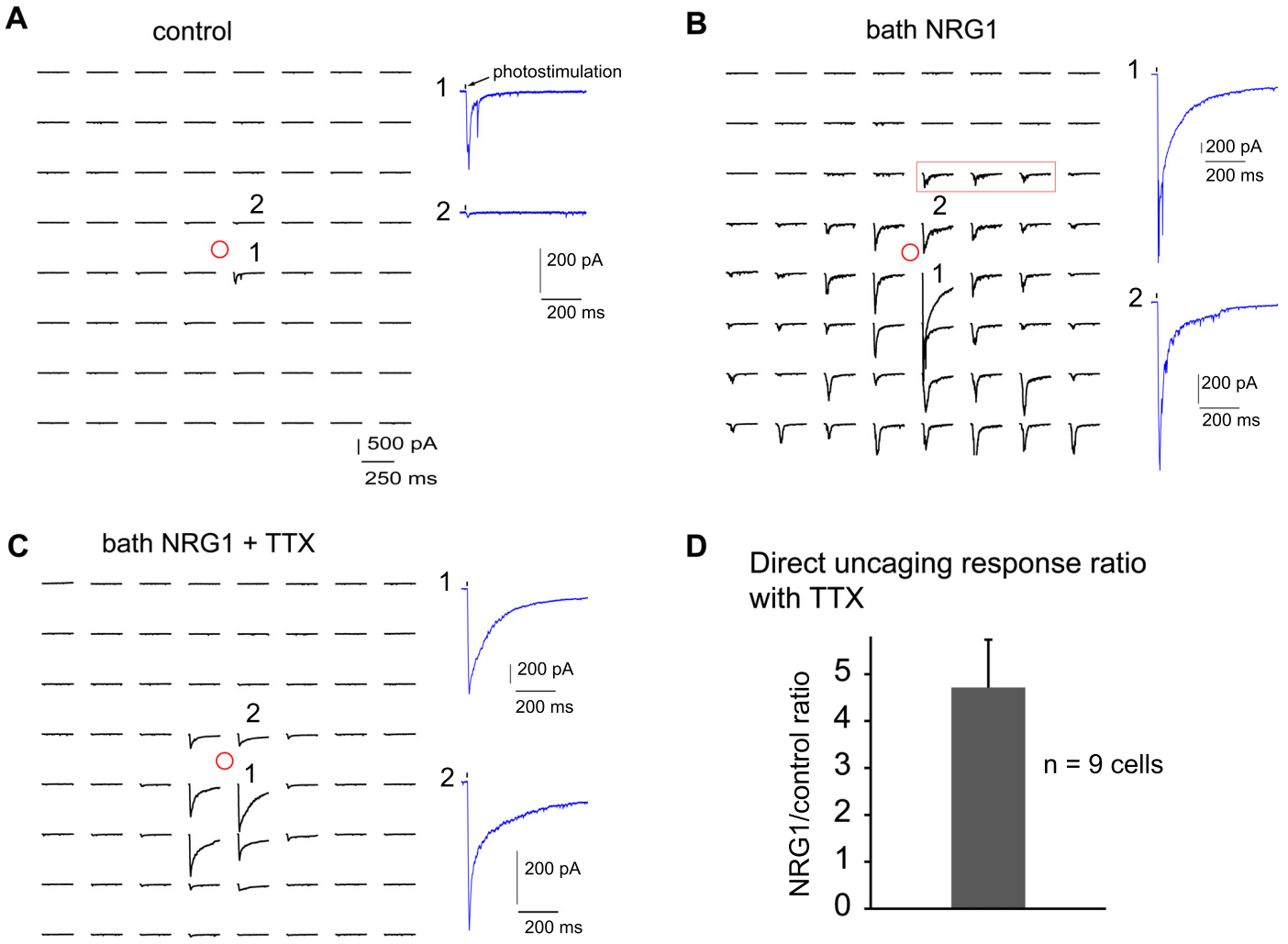

Supplementary Figure 5. NRG1 enhancement of direct uncaging responses of deprived PV neurons persists relative to control with the co-application of tetrodotoxin (TTX) that blocks neuronal action potentials and evoked synaptic inputs.

A-C. Example photostimulation data from a deprived PV neurons at control, bath applied NRG1 and the co-application of NRG1 and TTX. The response traces plotted from the photostimulation onset, were acquired from the mapping grid of 8 x 8 sites (65 μm^2 apart), centered at the recorded cell body (indicated by the red circle) at the specified conditions. The responses at the labeled perisomatic sites are expanded and shown separately by the panels. The TTX effect was confirmed by spiking block of the recoded neuron evoked by intrasomatic current injection. Note that the TTX co-application in **C** also blocks evoked synaptic inputs (examples within the red rectangle in **B**) to the recorded neurons. **D**. The bar graph shows the average direct uncaging response ratio (4.72 ± 1, n = 9 cells) of before and during bath application of NRG1 and TTX.

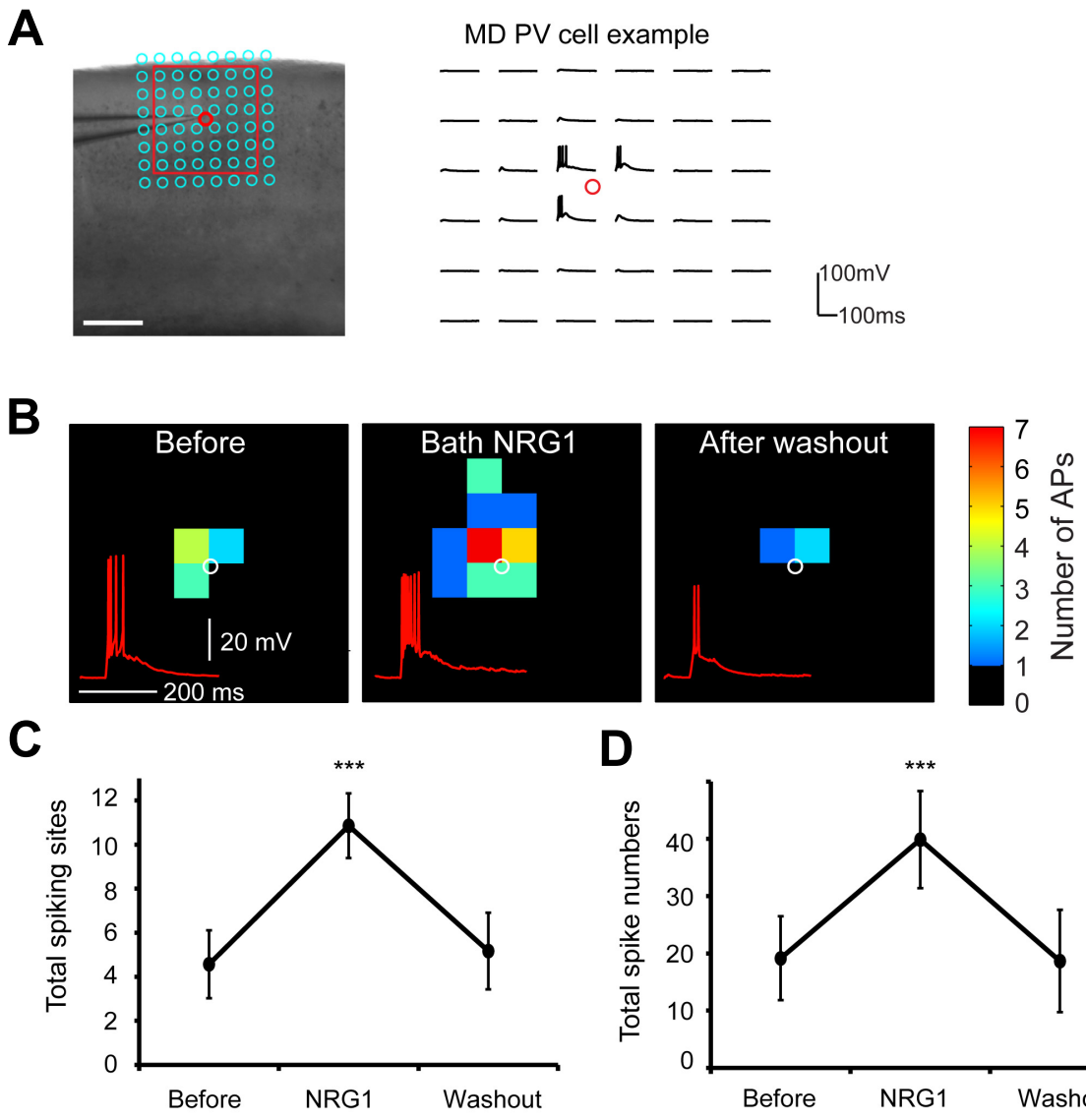

Supplementary Figure 6. NRG1 treatment increases glutamate evoked spiking of monocular deprived PV neurons.

A-B, Spiking activities through laser scanning photostimulation via glutamate uncaging are used to assess evoked excitability of PV neurons. **A,** Left: V1 slice image superimposed with photostimulation sites (cyan circles) spaced at 60 µm x 60 µm. The red circle indicates the tip of a recording electrode and the cell body location of a deprived PV neuron. Right: The plot of photostimulation responses from the recorded PV cells before bath NRG1 at the selected sites within the red square (left). Current clamp recording was used to examine suprathreshold spiking activities in PV neurons. **B**, NRG1 treatment increases glutamate evoked PV neuron excitability in terms of the number of spiking sites and total spike numbers per map, illustrated by the spiking maps recorded before, during and after washout of bath NRG1. The data shown in (**A**) and (**B**) are from the same PV neuron. Each colored square indicates a spiking site. Warmer colors indicate larger numbers of photostimulation evoked action potentials (AP). The inserted traces of spiking are from the uncaging site at the map center under different conditions. **C-D**, Plots of average total spiking sites (**C**) and total spike numbers (**D**) per map for a group of PV cells from monocular deprived animals (n = 7 cells) measured before, during and after washout of bath NRG1. Of 7 cells, 6 have complete data and one is lacking washout data. *** indicates the significance level of $p < 0.001$ between NRG1 responses versus baseline or washout (Mann–Whitney U tests).

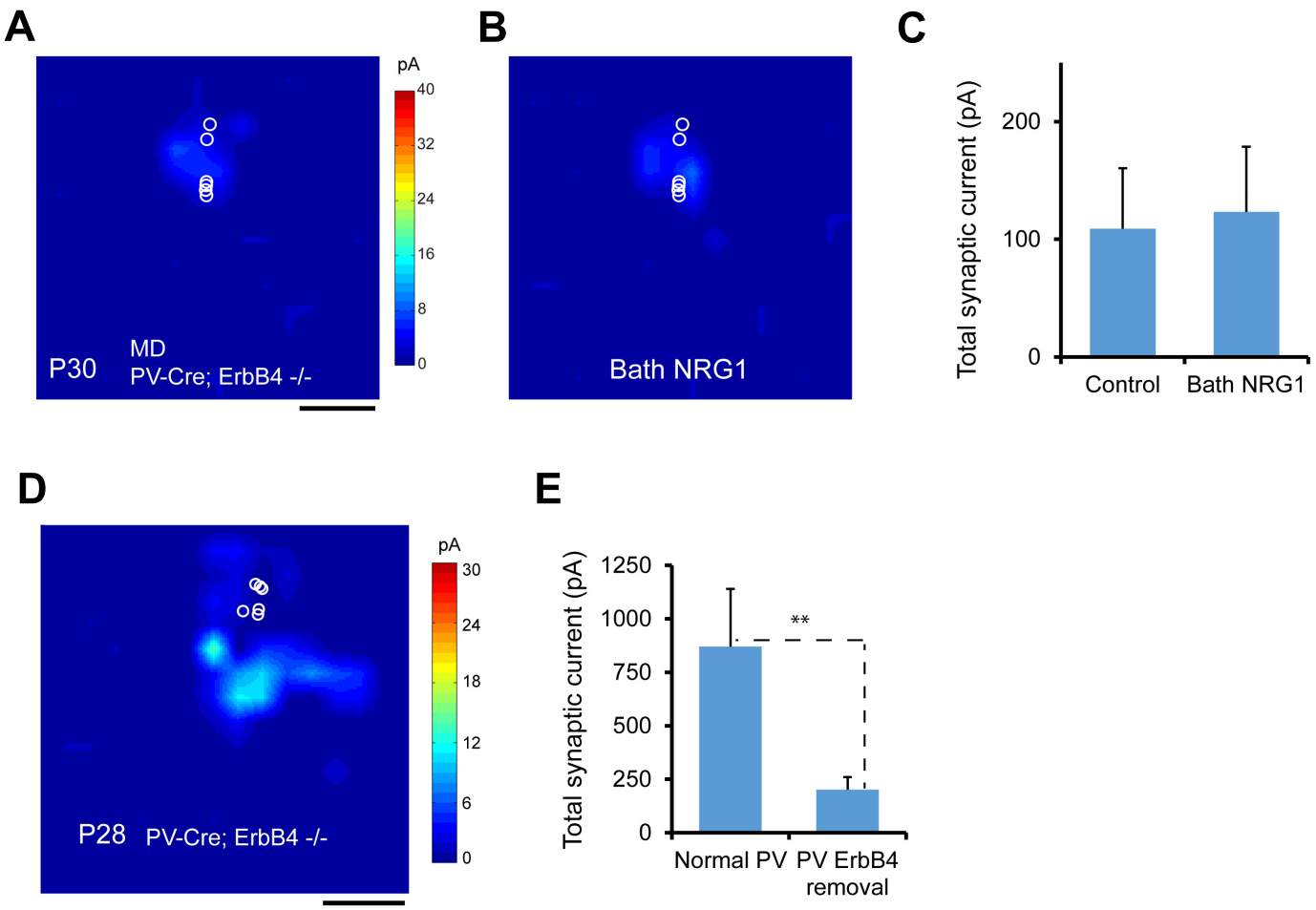

Supplementary Figure 7. ErbB4 genetic ablation abolishes NRG1 effects and reduces excitatory synaptic input to PV neurons.

A-C. Bath NRG1 has no effect on deprived PV neurons in PV-Cre+/-; ErbB4$^{flx/flx}$ mice in which ErbB4 is ablated specifically in PV neurons. **A** and **B** show quantitative group averaged, excitatory input maps before and during bath NRG1 of deprived L2/3 PV neurons (n = 6, P30-31), respectively. Scale = 200 µm. **C**, Summary data showing average total synaptic input strength measured from these neurons before and during bath NRG1 (Mann–Whitney U test, p = 0.9). **D-E.** Excitatory synaptic inputs to non-deprived PV neurons from local V1 circuits are reduced in PV-Cre+/-; ErbB4$^{flx/flx}$ mice. **D** shows the quantitative group averaged, excitatory input maps of P28 non-deprived L2/3 PV neurons (n = 6). Scale = 200 µm. **E**, Summary data showing that average total synaptic input strength measured from ErbB4 knockout PV neurons are weak compared with normal, non-ErbB4 knockout PV cells (n = 11). **, p = 0.02 (Mann–Whitney U test).

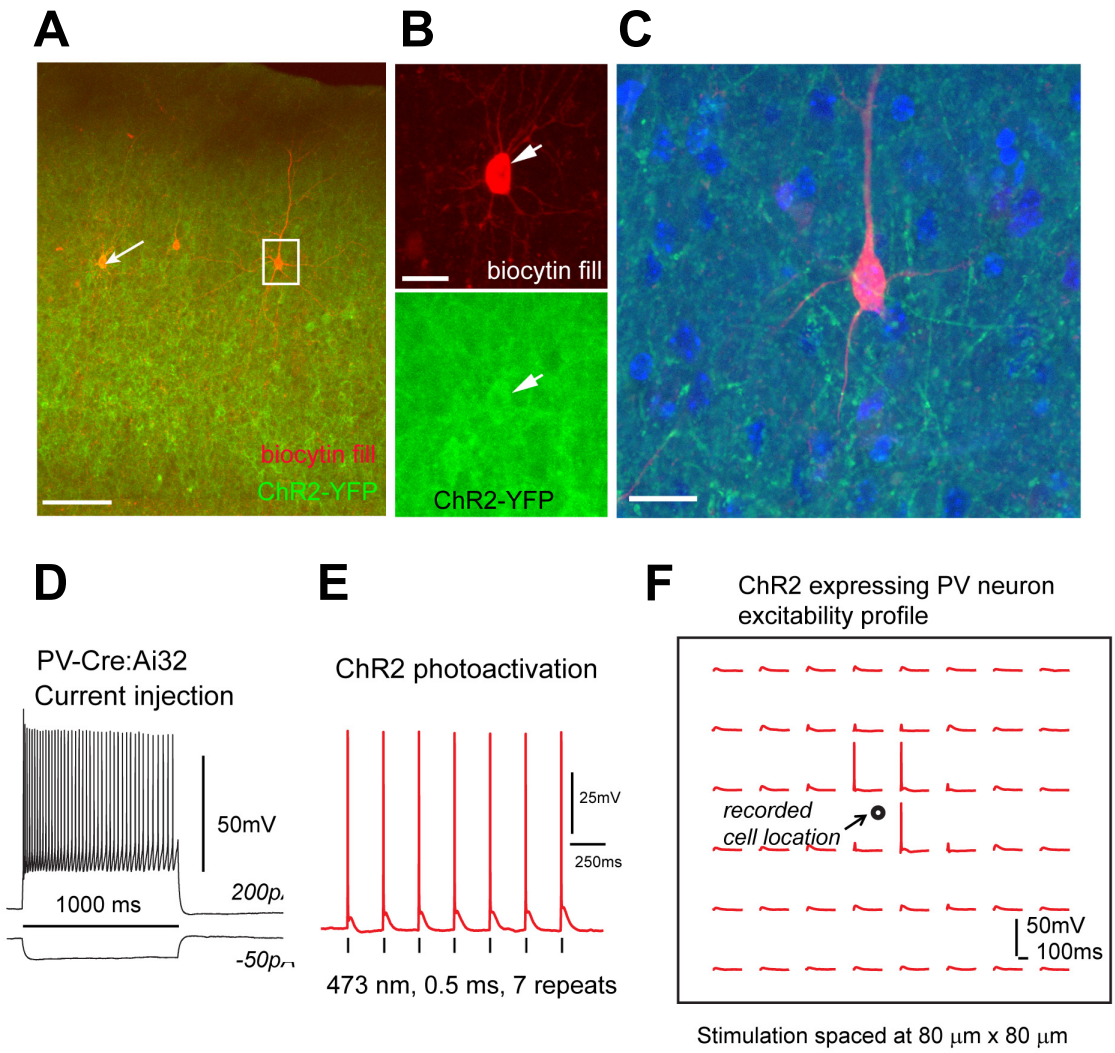

Supplementary Figure 8. Mapping PV-specific inhibitory inputs to excitatory neurons through optogenetic stimulation.

A-C, PV specific ChR2 expression is achieved through a Cre-directed approach by crossing the PV-Cre mouse to the Ai32 mouse with a Rosa-CAG-LSL-ChR2(H134R)-EYFP-WPRE conditional allele. **A**, Confocal image showing yellow fluorescent protein (YFP) fluorescence (i.e., ChR2-fused EYFP expression) (shown in green) of PV cell bodies and their dendrites/axons in a post-fixed PV-Cre; Ai32 mouse slice. The recorded neurons are post hoc identified based on their intrinsic electrophysiology and on morphology revealed by intracellular biocytin staining (red). The arrow indicates a PV fast-spiking neuron while the square indicates an excitatory pyramidal neuron. Scale = 100 μm. **B**, Recording from PV neurons is facilitated by detection of their YFP fluorescence in acutely cut PV-Cre; Ai32 mouse slices. **C**, The pyramidal neuron and many presumptive excitatory neurons (revealed by DAPI staining, blue) are surrounded by YFP positive, PV specific axonal processes. Scale = 20 μm **B**, **C**. **D-E**, Responses to intrasomatic current injections **D** and photoactivation **E**, 473 nm laser, 3 mW) of a ChR2-expressing PV neuron, respectively. **F**, The excitability profile of the ChR2+, PV neuron to photoactivation (0.25 ms, 3 mW) at the 5 x 6 sites (spaced at 80 μm^2) with 3 spiking sites close to the cell body location, which demonstrates good spatial precision of optogenetic stimulation under our experimental condition. The response traces are plotted for 200 ms beginning at photoactivation onset.

Supplemental Experimental Procedures

Animals

All experiment procedures and protocols were approved by the Institutional Animal Care and Use Committee of the University of California, Irvine. To genetically label parvalbumin-positive neurons, PV-IRES-Cre knock-in mice (Jackson Laboratories, West Grove, PA, stock #008069) were crossed with the Ai9 tdTomato reporter knock-in mice directly received from Jackson Laboratory (stock #007905). All experimental mice were hemizygous for both transgenes (PV-Cre; Ai9). Similarly, for immunochemical experiments (Supplementary Fig. 2), GABAergic cells were genetically labeled in GAD2-Cre; Ai9 mice, and inhibitory neurons expressing somatostatin and vasoactive intestinal peptides were labeled in SOM-Cre; Ai9 and VIP-Cre; Ai9 mice (Taniguchi et al., 2011). To control and compare tdTomato labeled PV cells, we also used a few G42 transgenic mice (Chattopadhyaya et al., 2004) in which most GFP-expressing cells are identified as parvalbumin-positive, fast-spiking basket cells. The NRG1 potentiation effect was similarly observed in deprived PV neurons in both PV-Cre; Ai9 and G42 mice. To enable PV specific mRNA expression analysis, PV-Cre mice were crossed to fsTRAP mice (Zhou et al., 2013) (Jackson Laboratory, stock #022367) to generate PV-Cre+/-; fsTRAP mice, in which translating polyribosomes of PV cells are tagged with EGFP from the GFP-L10 transgene. Similarly, EMX1-Cre mice were crossed to fsTRAP mice for targeting excitatory neurons for fsTRAP analysis. Emx1 is predominantly expressed in forebrain excitatory neurons (Gorski et al., 2002). To generate ErbB4 conditional knockout mice, the mice homozygous for loxP-flanked (flx) ErbB4 alleles (Long et al., 2003) were first crossed with PV-Cre mice. The resulting PV-Cre$^{+/-}$, ErbB4$^{flx/+}$ mice were then crossed back to the homozygous loxP-flanked ErbB4 mice to produce PV-Cre$^{+/-}$; ErbB4$^{flx/flx}$ mice. Wild-type C57/BL6 mice were obtained from Charles River Laboratories (San Diego, CA). The animals (2-5 per cage) were housed in a vivarium room with a 12-h light/dark cycle with access to food and water ad libitum.

Mice were randomly assigned to either control or monocular deprivation treatment groups. Monocular deprivation was performed under isoflurane/oxygen anesthesia (3% induction and 2% maintenance), antibacterial ointment applied to eyes, lid margins trimmed and one mattress suture (silk 6 or 4-O) was used to bind the upper and lower lids. Any mice showing signs of eye infection or lid separation were removed from the study. To enhance NRG1 signaling *in vivo* in the cortex following multiple-day monocular deprivation, some of the animals received subcutaneous administration (3 times (3x) daily, every 8 hours, 0.5 μg NRG1 per mouse) of recombinant human NRG1-β1 purchased from R&D systems (396-HB-050, 8 kDa, Minneapolis, MN). To compare the effects of bath administered NRG1 versus *in vivo* NRG1 treatment, 1-day monocular deprived mice were with subcutaneously administered recombinant NRG1 (single injection, 1 μg NRG1 per mouse). The animals were killed after one hour of NRG1 injection for electrophysiological experiments. The dosage of *in vivo* NRG1 treatment was determined based on our empirical evidence from electrophysiological experiments (Fig. 3) in conjunction with the relevant information from previous studies (Abe et al., 2011; Bersell et al., 2009).

In order to genetically target and label PV neurons in PV-Cre mice or PV-Cre; ErbB4$^{flx/flx}$ mice, we used Cre-dependent AAV-mediated viral expression of mCherry or hM4D-mCherry in these neurons. Mouse pups at P14 were anesthetized under isoflurane for stereotaxic viral injections. The scalp was retracted and a small burr hole was drilled over the left occipital pole overlying the binocular zone of primary visual cortex. A pulled glass pipette (tip diameter ~ 30 μm) was loaded with the AAV5-DIO-hM4D-mCherry or AAV5-DIO-mCherry (~ 2 x 10^{11} genome units/ml; UNC Vector Core, University of North Carolina at Chapel Hill) and then lowered into the brain, and a Picospritzer was used to pulse 0.1 μl virus into the binocular V1 region. The scalp was then sutured shut over the burr hole and the mouse was left for 2 weeks to enable high level mCherry or hM4D-mCherry expression. For DREADDs experiments, clozapine N-oxide (CNO) was injected i.p. (0.3 mg/kg, every 8 hours) to inhibit PV neuronal activity *in vivo* at P28 for 24 hours.

Based on published studies (Ellis et al., 2006; Johns et al., 2003; Nagane et al., 2001) and our control experiments, we chose to use intracerebroventricular (i.c.v.) delivery of an ErbB receptor tyrosine kinase inhibitor AG1478 (Cat. No. 658552, Calbiochem) in a sub-toxic dosage for the *in vivo* ErbB blockade experiments. Two micro-liters (μl) of 10 mM AG1478 dissolved in DMSO was injected via a glass pipette to block ErbB4 activation in the cortex of PV-Cre; Ai9 mice, matching our *in vitro* AG1478 experiments. We injected 2 μl of DMSO in littermate mice for control. The injection was performed with animals undergoing a short duration of isoflurane anesthesia. We did not observe abnormal behaviors or toxicity after AG1478 injection. Given the reported short half-life of in vivo AG1478 (Ellis et al., 2006), we divided the animals and let them survive for two different time points, 6 hours (n = 3 animals) and 20 hours (n = 3 animals) after AG1478 injection. While the 6 hr survival group appeared to have stronger reduction in NRG1 expression than the 20 hr survival group, both groups showed a consistent trend of reduced NRG1 expression relative to controls (n = 6 animals). The 6 and 20 hr data are pooled in the final figure (Fig. 2L) for format consistency with the other figures but the time point data detail is described above.

Immunohistochemistry

For immunochemical staining experiments, animals were deeply anesthetized with Uthasol (sodium pentobarbital, 100 mg/kg, i.p.) and transcardially perfused with 5 ml 0.1M phosphate buffered saline (PBS, pH 7.3–7.4), followed by 25 ml 0.1M PBS containing 4% paraformaldehyde and phosphatase inhibitor (PhosSTOP, 1 tablet for 20 ml, Roche, Switzerland). The brains were removed and left in 4% paraformaldehyde for 6-24 hours, then transferred into 30% sucrose in 0.1M PBS. The brains were sectioned coronally in 25 μm thickness on a freezing microtome (Leica SM2010R, Germany). Selected mouse V1 coronal sections from bregma -3.40 mm to -3.80 mm were used for immunochemical staining experiments and quantitative analysis. For animals having undergone the treatment of monocular deprivation, sections were taken from the hemisphere contralateral to the deprived eye.

Free-floating sections were rinsed 3-4 times with PBS, and incubated in a blocker solution for 1 hour at room temperature on the shaker. The blocker solution contains 5% normal donkey serum and 0.25% Triton X in PBS. Sections were then incubated with the primary antibody in the blocker solution at the appropriate dilution for 36 hours at 4 °C. After the primary antibody incubation, sections were rinsed thoroughly with PBS (or working buffer: 10% blocker and 90% PBS; 6 times), and incubated with an appropriate secondary antibody in the blocker solutions for 2 hours at room temperature. Once the secondary antibody solution was rinsed off, sections were counterstained with 10 μM 4'-6-diamidino-2- phenylindole (DAPI; Sigma-Aldrich, St. Louis, MO) for 10 minutes to help distinguish cortical laminar structures. Finally, sections were rinsed and wet-mounted, and were directly cover-slipped with the mounting medium Vectashield (H-1000, Vector, Burlingame, CA). Primary antibodies against ErbB4 (Rabbit polyclonal, 0618, provided by Dr. Cary Lai at Indiana University; 1:1000), NRG1 (Rabbit polyclonal, ab27303, Abcam, Cambridge, MA; RRID:AB_2154665; 1:300-1000), phospho-ErbB4 (Rabbit monoclonal, ab109273, Abcam; RRID:AB_10866384; 1:250), and phospho-tyrosine (Rabbit monoclonal, RM111, RevMAb; RRID:AB_2619618; 1:300) were used to examine specific immunochemical signals in primary visual cortex, followed with Alexa Fluor (AF) 488–conjugated donkey anti-rabbit (Jackson ImmunoResearch, West Grove, PA, 1:200) secondary antibody to visualize the staining. To identify parvalbumin (PV) positive neurons in wild type animals, the primary goat anti-PV antibody (PVG-213, Swant, Switzerland; RRID:AB_10000345; 1:1000) and the secondary Cy3-conjugated donkey anti-goat antibody (Jackson ImmunoResearch, 1:200) were used. Per Abcam technical information, the NRG1 antibody is specific to Type 1 isoforms; its specificity was verified through our immunoabsorption tests. We carried immunoabsorption control experiments by pre-incubating 1:1000 dilution of the NRG1 antibody (ab27303) with the recombinant human NRG1-β1 (R&D systems) (10 μg/ml) overnight first, and then adding the mixed antibody and NRG1 solution for subsequent immunochemical staining procedure. The specificity of ErbB4 and phospho-ErbB4 antibodies was confirmed in PV-Cre; ErbB4$^{flx/flx}$ mouse sections.

Immunostained sections were examined, and low- and high-power image stacks were acquired by using confocal microscopes (LSM 700 and LSM 780, Carl Zeiss Microscopy, Germany). Image tiles, overlaying, maximum projections, and subset z-stack selections were performed using the Zeiss image processing software. For quantitative fluorescence image analysis, all the sections of staining series were acquired using the same acquisition settings (e.g., laser powers, pinhole sizes, line scan numbers), and the data images were digitally processed in an identical manner. Individual cell fluorescence measurements (immunofluorescence) were performed in final output images using Adobe Photoshop software (CS4 extended version, Adobe Systems, San Jose, CA). L2/3 PV or putative excitatory neurons with clear somata in binocular V1 regions were selected; the cell areas (number of pixels) and their integrated density (whole cell fluorescence intensity) were measured. The background reading of the fluorescence level was determined for each stained V1 section image. Corrected total fluorescence per cell (Burgess et al., 2010) in arbitrary units (a.u.) was calculated in an Excel sheet by applying the measurements obtained from the analyzed cell with the formula: Corrected Total Cell Fluorescence (CTCF) = Integrated Density - (Area of selected cell X Mean fluorescence of background reading). For immunostaining fluorescence quantification, the staining intensity (measured by corrected total fluorescence) of PV and non-PV neurons from individual mice (1-2 sections per mouse) in each group were quantified; the mean values with all neurons per each mouse were calculated. Then these mean values were normalized to the specified mean for the control condition or age group in the same staining series. The overall normalized values from different mice were compared across different age groups or conditions (e.g., Figs. 1 and 2).

Purification of mRNA from fs-TRAP mice

Purification of polysomally bound mRNA from visual cortical lysate was performed as described with modifications (Zhou et al., 2013). Briefly, visual cortex was dissected in ice-cold ACSF (in mM: 126 NaCl, 2.5 KCl, 26 $NaHCO_3$, 2 $CaCl_2$, 2 $MgCl_2$, 1.25 NaH_2PO_4, and 10 glucose).

Pooled visual cortex from two to three mice was grinded to powder on dry ice, followed with sonication for 5 seconds in ice-cold lysis buffer [20 mM HEPES (pH 7.4), 150 mM KCl, 5 mM MgCl2, 0.5 mM dithiothreitol, 100 µg/ml cycloheximide (Sigma-Aldrich), protease inhibitors (Roche) and 40 U/ml recombinant RNase inhibitor (Promega, Madison, WI)]. Homogenates were centrifuged for 10 min at 2, 000x g, 4 °C, to pellet nuclei and large cell debris, and NP40 (Invitrogen, Carlsbad, CA) and DHPC (Avanti Polar Lipids, Alabaster, Alabama) were added to the supernatant at final concentrations of 1% (vol/vol) and 30 mM, respectively. After incubation on ice for 5 minutes, the lysate was centrifuged for 10 minutes at 20,000x g to pellet insoluble material. Two mouse monoclonal anti-GFP antibodies, Htz-GFP19C8 and Htz-GFP19F7 (50 µg each, Memorial Sloan-Kettering Monoclonal Antibody Facility, New York, NY) were added to bind to 375 µl protein G Dynal magnetic beads (Invitrogen). Alternatively, 300 µl of the streptavidin Myone T1 dynabeads were binding to 120 µl 1 µg/µl biotinylated protein L first, then followed with two mouse monoclonal anti-GFP antibodies incubation. After being washed twice with the polysome extraction buffer, the beads were then added to the cell-lysate supernatant, and the mixture was incubated at 4 °C with end-over-end rotation for 30 minutes. The beads were subsequently collected on a magnetic rack and washed four times with high-salt polysome wash buffer [20 mM HEPES (pH 7.4), 350 mM KCl, 5 mM MgCl2, 1% NP-40, 0.5 mM dithiothreitol and 100 µg/ml cycloheximide]. RNA was eluted from the beads by incubating beads in RLT buffer (Rneasy Micro Kit, Qiagen, Venlo, Netherlands) with β-mercaptoethanol (10 µl/ml) for 5 minutes at room temperature. Eluted RNA was purified using RNeasy Micro Kit (Qiagen) per the manufacturer's instructions including in-column DNase digestion. Immunoprecipitated RNA yield for each sample was approximately 3 ng/µl.

Western blotting

To confirm the specificity of Cre-dependent expression of GFP-L10a fusion protein (Supplementary Fig. 2), the bead elution was subjected to denaturing NuPAGE Tris-acetate gel

(Invitrogen) electrophoresis and then electrophoretically transferred to nitrocellulose membranes. Five percent low-fat milk in phosphate-buffered saline containing 0.1% Tween-20 was used to block nonspecific binding for at least 1 hour at room temperature. The mouse monoclonal anti-GFP antibodies (Htz-GFP19C8 and Htz-GFP19F7GFP) in phosphate-buffered saline were incubated with the membranes at 4°C for overnight. The antibody-protein complexes were visualized by chemiluminescent reagents.

Quantitative PCR

Purified RNA (30 ng) was used to produce cDNA with a SuperScript® III First-Strand Synthesis SuperMix Kit for RT-qPCR (Invitrogen) following the manufacturer's instructions. Resulting cDNA was used to perform the quantitative PCR with Platinum SYBR Green qPCR SuperMix (Invitrogen), with 500 nM final concentration of each primer. Cycling and quantitation was performed with ViiA^{TM} 7 Real-Time PCR System (Applied Biosystems, Waltham, MA) using the VIIATM 7 software v1.2. PCR was carried out for 2 min 50 °C, 5 min 95 °C, 40 cycles (15 seconds for 95°C, 30 seconds for 50°C), followed by a melt curve. Each replicate was assayed in sixplicate. Gene expression was normalized to gapdh and presented as mean ± SEM. The following primers were used: ErBb-4-fwd CATGGCCTTCCAACATGACTCTGG, ErBb-4-rev GGCAGTGATTTTCTGTGGGTCCC; NrG1-I/II-fwd GGCAGTGATTTTCTGTGGGTCCC, NrG1-I/II -rev GGCAGTGATTTTCTGTGGGTCCC; gapdh-fwd TGCCAACATCACCATTGTTGA, gapdh -rev TGCCAACATCACCATTGTTGA. For fold enrichment in TRAP, the target gene was normalized to Gapdh in both input and TRAP fractions [i.e., fold TRAP enrichment = 2(ΔCt_target – ΔCt_gapdh)].

Electrophysiology and Laser Scanning Photostimulation

Coronal sections of 400 μm were cut from primary visual cortex (V1) with a vibratome (VT1200S, Leica Biosystems, Buffalo Grove, IL) in sucrose containing ACSF (in mM: 85 NaCl, 75 sucrose, 2.5 KCl, 25 glucose, 1.25 NaH_2PO_4, 4 $MgCl_2$, 0.5 $CaCl_2$, and 24 $NaHCO_3$). For animals

having undergone monocular deprivation, sections were taken exclusively from the hemisphere contralateral to the deprived eye. Slices were incubated for at least 30 minutes in normal ACSF (in mM: 126 NaCl, 2.5 KCl, 26 $NaHCO_3$, 2 $CaCl_2$, 2 $MgCl_2$, 1.25 NaH_2PO_4, and 10 glucose) at 32 °C before transferred into slice recording chambers. Throughout the cutting, incubation and recording, the solutions were continuously supplied with 95% O_2–5% CO_2.

Whole cell recordings were performed under a DIC/fluorescent Olympus microscope (BX51WI, Olympus, Japan). Oxygenated ACSF at room temperature was perfused into the slice recording chamber through a custom-designed flow system driven by pressurized 95% O_2–5% CO_2 (3 PSI) at roughly 2 mL/min. Slices were examined under a 4x objective for proper targeting of either L2/3 PV interneurons that express red fluorescent proteins (RFP), tdTomato or excitatory pyramidal neurons within binocular regions of mouse V1 using landmarks defined in reference (Antonini et al., 1999). To target whole cell recordings, cells were visualized at high magnification (60X objective, 0.9 NA; LUMPlanFl/IR, Olympus). Cell bodies of recorded neurons were at least 50 μm below the surface of the slice. Patch pipettes (4 – 6 MΩ resistance) made of borosilicate glass were filled with an internal solution containing (in mM) 126 K-gluconate, 4 KCl, 10 HEPES, 4 ATP-Mg, 0.3 GTP-Na, and 10 phosphocreatine (pH 7.2, 300 mOsm). For the recordings in which IPSCs were measured, potassium was replaced with cesium. Electrodes also contained 0.1% biocytin for post-hoc cell labeling and further morphological identification. Once stable whole-cell recordings were achieved with good access resistance (usually <30 MΩ), basic electrophysiological properties were examined through hyperpolarizing and depolarizing current injections. For intracellular application experiments of PKC inhibitory peptides (PKC 19-36, Tocris, 10 μmol/L in the internal solution of recording pipettes) and light chains of botulinum toxin type B (BTX) (List Biological Laboratories, Campbell, CA; 2 μg/mL in the internal solution), we waited for 15 minutes after the neurons were recorded to allow the respective reagents to infuse into the recorded cells for full effects. For protein synthesis inhibition experiments, slices were pre-incubated in 50 μM anisomycin (a peptidyl transferase inhibitor, Sigma-Aldrich) (Huber et al.,

2000; Ramiro-Cortes and Israely, 2013) for 30 minutes before experiments of bath administrated NRG1. Electrophysiological data were acquired with a Multiclamp 700B amplifier (Molecular Devices, Sunnyvale, CA), data acquisition boards (models PCI MIO 16E-4 and 6713, National Instruments, Austin, TX), and custom modified version of Ephus software (Suter et al., 2010). Data were digitized at 10 kHz. Any recordings in which the access resistance changed by >20% during the course of the experiment were excluded from analysis.

PV inhibitory neurons were targeted based on RFP expression and verified by fast spiking patterns from current injections. Excitatory neurons were selected based upon their pyramidal somata detected under differential interference contrast (DIC) microscopy; they were RFP negative, and showed regular spiking patterns to suprathreshold intrasomatic current injections. Final cell type classification was determined by the combined characterization of RFP expression, electrophysiological and morphological properties of the recorded cells. The morphology of each recorded neuron was determined using post-hoc staining. Briefly, brain slices were fixed in 4% paraformaldehyde and transferred to 30% sucrose solution in PBS. Neurons filled with biocytin during recordings were labeled with Alexa Fluor 488-conjugated streptavidin (1:500 dilution; Jackson ImmunoResearch). Slices were also stained for DAPI to identify laminar boundaries. Cell morphology, DAPI labeling, and RFP expression were visualized using an Olympus BX61 epifluorescent microscope and MetaMorph imaging suite (Molecular Devices).

Laser scanning photostimulation (LSPS) was performed through a 4x objective lens. Stock solution of MNI-caged-l-glutamate (Tocris Bioscience, United Kingdom) was added to 20 ml of ACSF for a concentration of 0.2 mM caged glutamate. The cortical slice image, acquired through the 4x objective, was visualized using a high-resolution digital CCD camera, and this image, in turn, was used to guide and register photostimulation sites. Photostimulation (1.5 ms duration, 15 mW pulses) from a 350nm UV laser generator (DPSS Lasers, Santa Clara, CA) was delivered to the sample, controlled via an electro-optical modulator and a mechanical shutter. Focal laser spots approximated a Gaussian profile with a diameter of ~100 μm. Under our

experimental conditions, LSPS evoked action potentials were recorded from stimulation locations within 88 ± 11 μm (n = 16) of targeted somata of excitatory neurons and occurred within 150 ms post photostimulation. Together with control experiments (Xu et al., 2010), our calibration analysis indicates that LSPS allows for mapping direct synaptic inputs to recorded neurons. Synaptic currents in patched neurons were detected under voltage clamp. By systematically surveying synaptic inputs from hundreds of different sites across a large cortical region, aggregate synaptic input maps were generated for individual neurons. For our mapping experiments, a standard stimulus grid (16×16 stimulation sites, 65 μm^2 spacing) was used to tessellate V1 from pia to white matter. The LSPS site spacing was empirically determined to capture the smallest predicted distance in which photostimulation differentially activates adjacent neurons. Glutamate uncaging was delivered sequentially in a nonraster, nonrandom sequence, following a "shifting-X" pattern designed to avoid revisiting the vicinity of recently stimulated sites (Shepherd et al., 2003). Because glutamate uncaging agnostically activates both excitatory and inhibitory neurons, we empirically determined the excitatory and inhibitory reversal potentials in L2/3 pyramidal cells to properly isolate EPSCs and IPSCs. We voltage clamped PV and pyramidal cells at -70 mV to determine LSPS evoked EPSCs.

Photostimulation induces two forms of excitatory responses: (1) those that result from direct activation of the recorded neuron's glutamate receptors, and (2) synaptically mediated responses (EPSCs) resulting from the suprathreshold activation of presynaptic excitatory neurons. Responses that occur within 10 ms of laser pulse onset were considered direct; these responses exhibited a distinct waveform and occurred immediately after glutamate uncaging (Fig. 2A; Supplementary Fig. 6C). Synaptic currents with such short latencies are not possible because they would have to occur before the generation of action potentials in photostimulated neurons. Therefore, direct responses were excluded from local synaptic input analysis, but they were used to assess glutamate mediated excitability/responsiveness of recorded neurons. At some locations, synaptic responses were over-riding on the relatively small direct responses, and these

responses were identified and included in synaptic input analysis. For data map analysis, we implemented the approach for detection and extraction of photostimulation-evoked postsynaptic current responses described in reference (Shi et al., 2010). LSPS evoked EPSCs were quantified across the 16x16 mapping grid for each cell, and 2 to 4 individual maps were averaged per recorded cell, reducing the likelihood of incorporating noise events in the analysis window. The EPSC input from each stimulation site was the measurement of the sum of individual EPSCs within the analysis window (>10 ms to 160 ms post photostimulation), with the baseline spontaneous response subtracted from the photostimulation response of the same site. The value was normalized with the duration of the analysis window (i.e., 150 ms) and expressed as average integrated amplitudes in picoamperes (pA). The analysis window was chosen because photostimulated neurons fire most of their action potentials during this time. For the color-coded map display, data were plotted as the average integrated EPSCs amplitude per pixel location (stimulation site) (e.g., Supplementary Fig. 6), with the color scale coding input strength. For the group maps obtained across multiple cells (e.g., Fig. 3), the individual cell maps were first aligned by their slice images using laminar cytoarchitectonic landmarks. Then a new map grid was created to re-sample and average input strength at each site location across cell maps; a smooth version of color-coded map was presented for overall assessments. To further quantitatively compare input strength across cell groups or different conditions, we measured the total ESPC inputs across all map sites (total synaptic input strength) for individual cells.

For the experiments that examined the effects of bath application of NRG1, AG1478 and CPP (Tocris Bioscience), the reagent(s) was/were added into the recording solution with specified concentrations. The drug application for 20 minutes was estimated to produce full effects, while the washout of 30 minutes was considered to remove the added drug from the recording solution.

Laser Scanning ChR2 Photoactivation

Similar to LSPS, we mapped PV specific inhibitory connections to excitatory neurons using laser scanning ChR2 photoactivation. This was achieved with PV inhibitory cell type-specific

optogenetic stimulation. The PV-Cre mouse line is crossed to the Ai32 mouse line (Madisen et al., 2012) that has a conditional allele of Rosa-CAG-LSL-ChR2(H134R)-EYFP-WPRE, to drive ChR2/EYFP fusion protein expression in PV cells. Whole cell recordings were made from layer 2/3 pyramidal neurons in binocular visual cortex of PV-Cre; Ai32 mice; spatial maps of PV cell connectivity strength to each patched pyramidal neuron were derived by systematically stimulating ChR2-expressing PV cells at 16 x 16 different sites arranged in a mapping grid across all cortical layers. Spatially restricted optogenetic activating of ChR2-expressing PV cells was accomplished using a 473 nm blue laser (3 mW, 0.25ms; laser spot diameter, ~50 μm). During optogenetic stimulation experiments, the ionotropic glutamate receptor antagonists [10 μM 6-cyano-7-nitroquinoxaline-2,3-dione (CNQX) and 5 μM CCP] were added to the bath solution to block excitatory synaptic input (GABAergic transmission is unaffected) and to avoid any potential dis-inhibition effects. Because interneurons can be interconnected by electrical synapses, we blocked gap junctions using 100 μM carbenoxolone. The reagents were purchased from Tocris Bioscience. Whole-cell voltage-clamp recordings were made from the recorded pyramidal neurons to measure ChR2-evoked inhibitory post-synaptic currents at the empirically determined holding potential at +5 mV with cesium-containing internal solution. The data analysis was similar to that described above for LSPS.

We have validated the effectiveness of our approach. Following high ChR2 expression in the cortex of the cross-bred pups (PV-Cre; Ai32), living brain slices were prepared and whole cell recordings were performed from ChR2/YFP-expressing PV cells that exhibited robust photoactivation-evoked spikes to repeated laser flashes (473 nm, 3 mW) (Supplementary Fig. 8). As ChR2-expressing PV cells only fired action potentials to blue laser photoactivation (0.25 ms, 3 mW) close to the cell body, we find that ChR2 photoactivation had sufficient spatial precision for laminar circuit mapping.

For electrical stimulation experiments shown in Fig. 7A-C, we recorded inhibitory post-synaptic current responses from L2/3 pyramidal neurons while a concentric bipolar electrode

(FHC Inc., Bowdoin, ME) connected to a stimulus isolator (World Precision Instruments, Inc., Sarasota, FL) was placed in L4 and used to preferentially activating L4 excitatory projections to L2/3 PV neurons.

Transcranial Intrinsic Signal Optical Imaging

We used both wild type C57BL/6 and PV-Cre$^{+/-}$; ErbB4$^{flx/flx}$ mice. There are technical caveats for using the PV-Cre; ErbB4$^{flx/flx}$ mice for *in vivo* studies. Since PV gene expression starts around 2 weeks postnatally, deletion of the ErbB4 gene in PV cells using the PV-Cre; ErbB4$^{flx/flx}$ crossing does not begin to reduce ErbB4 receptor levels until this developmental time point. Although our circuit mapping experiments shows reduced circuit inputs to L2/3 PV neurons in the visual cortex of PV-Cre; ErbB4$^{flx/flx}$ mice, in this genetic condition, our control experiments indicate that ErbB4 is reduced but not eliminated during the in vivo experimental time (4 day MD between P27-P31). In addition, high expression levels of ErbB4 are known in both developing and adult retinas (Bermingham-McDonogh et al., 1996). Thus, genetic knockouts of ErbB4 in the retina in the PV-Cre; ErbB4$^{flx/flx}$ mice may affect the light-activated responses of peripheral retinal neurons. Compromised retinal function would in turn complicate our interpretation of the effects of visual deprivation from in vivo imaging. However, no differences in the cortical responses to visual stimulation are observed between PV-specific ErbB4 knockout (PV-ErbB4 KO) mice and their control littermates before monocular deprivation. The overall contralateral cortical responses (in the unit of $\Delta R/R \times 10^4$) in PV-ErbB4 KOs (n = 4) and their control littermates (n = 6) are 1.5 ± 0.28 (mean ± SE) and 1.39 ± 0.1, respectively ($p = 0.96$, Mann-Whitney U test). The overall ipsilateral cortical responses in PV-ErbB4 KOs and their control littermates are 0.99 ± 0.16 (mean ± SE) and 0.96 ± 0.09, respectively ($p > 0.99$). Although we find that ocular dominance plasticity is impaired in PV-ErbB4 KOs, these data indicate that ablating the ErbB4 receptors specifically in PV interneurons does not perturb the overall cortical responses up to the age tested (P26).

All mice, with treatments blinded for the operator, were anesthetized with isoflurane in O2 (2%-3% for induction; 1.5% for surgical procedures; 0.6%-0.9% for imaging). During imaging

sessions, anesthesia was supplemented by a single intraperitoneal injection of chlorprothixene (1 - 2.5 mg/kg). Atropine (0.3 - 1 mg/kg) and carprofen (5 mg/kg) were administered subcutaneously to reduce secretions and to provide analgesia, respectively. Body temperature was maintained at 37.5°C using a feedback controlled homeothermic heating pad. For imaging, the skull over right visual cortex was exposed and covered with agarose (1.5% w/V in 1X PBS) and a coverslip. Agarose was sealed using sterile ophthalmic ointment (83% white petrolatum, 15% mineral oil; Rugby Laboratories, Livonia, MI) to prevent drying. Eyelashes were trimmed and a thin coat of silicone oil (30,000 cSt; Dow Corning, Midland, MI) was placed over the eyes for protection during imaging.

A SciMedia THT macroscope (Leica PlanApo 1.0X; 3.4 mm x 3.4 mm image area) equipped with an Andor Zyla sCMOS camera was used to collect visual response data. The surface vasculature was visualized using a 530 nm LED light with the camera focused on the cortical surface (LED4D210, Thorlabs, Newton, NJ). For intrinsic signal recording, illumination was changed to 617 nm LED light and the camera was focused ~600 μm beneath the pial surface. Custom written Matlab (Mathworks, Natick, MA) code was used to acquire images and stream to disk.

Visual stimuli were generated by custom-written Matlab code using the Psychophysics Toolbox. The monitor was positioned 25 centimeters from the animal and covered with a color correction gel filter sheet (day blue gel D2-70; Lowel, Hauppauge, NY) to better exploit the spectral sensitivity of mouse vision. A visual sweeping noise stimulus was created by multiplying a band limited (<0.05 cyc/deg; <2 Hz) spatiotemporal noise movie with a one dimensional Gaussian spatial mask (30 degrees) whose position swept across the monitor every ten seconds. Stimuli were presented on an Asus VG248 monitor (30 cm × 53 cm, 144 Hz refresh rate, 35 cd/m2 mean luminance). To generate retinotopic response maps, we presented this visual noise stimulus periodically sweeping from –18 to 36 degrees or from 36 to -18 degree visual field elevation. The screen was centered in front of the animal. To measure ocular dominance

responses, visual stimulation was limited to the binocular visual field (-10 degree to +20 degree visual field azimuth). Responses in the visual cortex were measured during stimulus presentation to the contralateral or the ipsilateral eye independently (stimulation of the other eye was prevented by blocking vision with a black plastic occluder). One recording session consisted of a stimulus being presented for 5 minutes to one eye. Sets of recordings were made in both directions 4-6 times per eye for a total of 40-60 minutes.

Maps of amplitude and phase of cortical responses were extracted from optical imaging movies via Fourier analysis of each pixel at the frequency of stimulus repetition (0.1 Hz) using custom written Matlab code. Overall map amplitude was computed by taking the maximum of the Fourier amplitude map smoothed with a 5 x 5 Gaussian kernel. Ocular dominance index (ODI) was computed as ODI = (C-I)/(C+I) where C and I are the averaged map amplitudes calculated for contralateral and ipsilateral visual stimulation respectively. Ocular dominance shift (ODS) was calculated for each animal in the adult MD experiments as ODS = (post-MD ODI – pre-MD ODI).

References for Supplemental Experimental Procedures

Abe, Y., Namba, H., Kato, T., Iwakura, Y., and Nawa, H. (2011). Neuregulin-1 signals from the periphery regulate AMPA receptor sensitivity and expression in GABAergic interneurons in developing neocortex. J Neurosci *31*, 5699-5709.

Antonini, A., Fagiolini, M., and Stryker, M.P. (1999). Anatomical correlates of functional plasticity in mouse visual cortex. J Neurosci *19*, 4388-4406.

Bermingham-McDonogh, O., McCabe, K.L., and Reh, T.A. (1996). Effects of GGF/neuregulins on neuronal survival and neurite outgrowth correlate with erbB2/neu expression in developing rat retina. Development *122*, 1427-1438.

Bersell, K., Arab, S., Haring, B., and Kuhn, B. (2009). Neuregulin1/ErbB4 signaling induces cardiomyocyte proliferation and repair of heart injury. Cell *138*, 257-270.

Burgess, A., Vigneron, S., Brioudes, E., Labbe, J.C., Lorca, T., and Castro, A. (2010). Loss of human Greatwall results in G2 arrest and multiple mitotic defects due to deregulation of the cyclin B-Cdc2/PP2A balance. Proc Natl Acad Sci U S A *107*, 12564-12569.

Chattopadhyaya, B., Di Cristo, G., Higashiyama, H., Knott, G.W., Kuhlman, S.J., Welker, E., and Huang, Z.J. (2004). Experience and activity-dependent maturation of perisomatic GABAergic innervation in primary visual cortex during a postnatal critical period. J Neurosci *24*, 9598-9611.

Ellis, A.G., Doherty, M.M., Walker, F., Weinstock, J., Nerrie, M., Vitali, A., Murphy, R., Johns, T.G., Scott, A.M., Levitzki, A.*, et al.* (2006). Preclinical analysis of the analinoquinazoline AG1478, a specific small molecule inhibitor of EGF receptor tyrosine kinase. Biochem Pharmacol *71*, 1422-1434.

Gorski, J.A., Talley, T., Qiu, M., Puelles, L., Rubenstein, J.L., and Jones, K.R. (2002). Cortical excitatory neurons and glia, but not GABAergic neurons, are produced in the Emx1-expressing lineage. J Neurosci *22*, 6309-6314.

Huber, K.M., Kayser, M.S., and Bear, M.F. (2000). Role for rapid dendritic protein synthesis in hippocampal mGluR-dependent long-term depression. Science *288*, 1254-1257.

Johns, T.G., Luwor, R.B., Murone, C., Walker, F., Weinstock, J., Vitali, A.A., Perera, R.M., Jungbluth, A.A., Stockert, E., Old, L.J.*, et al.* (2003). Antitumor efficacy of cytotoxic drugs and the monoclonal antibody 806 is enhanced by the EGF receptor inhibitor AG1478. Proc Natl Acad Sci U S A *100*, 15871-15876.

Long, W., Wagner, K.U., Lloyd, K.C., Binart, N., Shillingford, J.M., Hennighausen, L., and Jones, F.E. (2003). Impaired differentiation and lactational failure of Erbb4-deficient mammary glands identify ERBB4 as an obligate mediator of STAT5. Development *130*, 5257-5268.

Madisen, L., Mao, T., Koch, H., Zhuo, J.M., Berenyi, A., Fujisawa, S., Hsu, Y.W., Garcia, A.J., 3rd, Gu, X., Zanella, S.*, et al.* (2012). A toolbox of Cre-dependent optogenetic transgenic mice for light-induced activation and silencing. Nat Neurosci *15*, 793-802.

Nagane, M., Narita, Y., Mishima, K., Levitzki, A., Burgess, A.W., Cavenee, W.K., and Huang, H.J. (2001). Human glioblastoma xenografts overexpressing a tumor-specific mutant epidermal growth factor receptor sensitized to cisplatin by the AG1478 tyrosine kinase inhibitor. J Neurosurg *95*, 472-479.

Ramiro-Cortes, Y., and Israely, I. (2013). Long lasting protein synthesis- and activity-dependent spine shrinkage and elimination after synaptic depression. PLoS One *8*, e71155.

Shepherd, G.M., Pologruto, T.A., and Svoboda, K. (2003). Circuit analysis of experience-dependent plasticity in the developing rat barrel cortex. Neuron *38*, 277-289.

Shi, Y., Nenadic, Z., and Xu, X. (2010). Novel use of matched filtering for synaptic event detection and extraction. PLoS ONE *5*, e15517.

Suter, B.A., O'Connor, T., Iyer, V., Petreanu, L.T., Hooks, B.M., Kiritani, T., Svoboda, K., and Shepherd, G.M. (2010). Ephus: multipurpose data acquisition software for neuroscience experiments. Front Neural Circuits *4*, 100.

Taniguchi, H., He, M., Wu, P., Kim, S., Paik, R., Sugino, K., Kvitsiani, D., Fu, Y., Lu, J., Lin, Y.*, et al.* (2011). A resource of Cre driver lines for genetic targeting of GABAergic neurons in cerebral cortex. Neuron *71*, 995-1013.

Xu, X., Olivas, N.D., Levi, R., Ikrar, T., and Nenadic, Z. (2010). High precision and fast functional mapping of cortical circuitry through a novel combination of voltage sensitive dye imaging and laser scanning photostimulation. J Neurophysiol *103*, 2301-2312.

Zhou, P., Zhang, Y., Ma, Q., Gu, F., Day, D.S., He, A., Zhou, B., Li, J., Stevens, S.M., Romo, D.*, et al.* (2013). Interrogating translational efficiency and lineage-specific transcriptomes using ribosome affinity purification. Proc Natl Acad Sci U S A *110*, 15395-15400.